

## Contrast enhancement of time-averaged fringes based on moving average mapping functions

Minvydas Ragulskis<sup>a,\*</sup>, Algimantas Aleksa<sup>a</sup>, Rimas Maskeliunas<sup>b,1</sup>

<sup>a</sup> Research Group for Mathematical and Numerical Analysis of Dynamical Systems, Kaunas University of Technology, Studentu 50-222, Kaunas LT-51638, Lithuania

<sup>b</sup> Department of Printing Machines, Vilnius Gediminas Technical University, J. Basanaviciaus 28-129, Vilnius LT-03224, Lithuania

### ARTICLE INFO

#### Article history:

Received 1 February 2008

Received in revised form

5 January 2009

Accepted 26 February 2009

Available online 8 April 2009

#### Keywords:

Moiré fringes

Contrast enhancement

Mapping function

Averaging in time

Dynamic deflections

### ABSTRACT

Moving average contrast enhancement techniques are applied for visualization of time-averaged fringes produced by time average projection moiré. The complexity of the problem is based on the fact that grayscale levels at centerlines of fringes depend from the geometrical location of these fringes. Moreover, moiré grating geometry determines the direction of sensitivity to dynamic deflections. Standard fringe visualization methods fail to produce interpretable results. The developed pixel-based analysis techniques enable efficient reconstruction of projected fringes.

© 2009 Elsevier Ltd. All rights reserved.

### 1. Introduction

Since moving average filters were introduced in signal processing few decades ago [1], a vast variety of nonlinear filters and families of nonlinear filters for image processing has been suggested. Main assumptions that constitute the suggested unified and structured treatment of nonlinear filters are [2]:

- (i) Filtering is performed within a filter window.
- (ii) In each position of the window, a certain estimation operation is applied to the neighborhood of the window central pixel.
- (iii) The neighborhood is formed on the base of window sample attributes (like rank, cardinality, spacial connectedness, etc.). The process of forming neighborhood may, in general, be a multi-stage one beginning from the initial neighborhood formed from filter window pixels through a series of intermediate neighborhoods.
- (iv) Intermediate neighborhoods may, in addition to its pixel attributes, have attributes associated with the neighborhood as a whole and obtained through an estimation operation over the neighborhood.
- (v) Nonlinear filters can be specified in terms of neighborhood forming and estimation operations they use.

Moving average, or low-pass filters usually take a form of some sort of moving window operator [3]. That operator usually affects one pixel of the image at a time, moving over the image to affect all the pixels in the image. Some common types are [4]:

- (i) Neighborhood-averaging filters: these filters replace the value of each pixel by a weighted-average of the pixels in some neighborhood around it. If all the weights are equal then this is a mean filter.
- (ii) Median filters: these filters replace each pixel value by the median of its neighbors, i.e. the value such that 50% of the values in the neighborhood are above, and 50% are below. This method is generally very good at preserving edges.
- (iii) Mode filters: each pixel value is replaced by its most common neighbor. These filters are particularly useful for classification procedures.

The above filters are all space invariant. The same operation is applied to each pixel location. A non-space invariant filtering can be obtained by changing the type of filter or the weightings used for the pixels for different parts of the image.

Image restoration from degraded images lies at the foundation of image processing, pattern recognition, and computer vision. A large number of image restoration filters have been devised so far. However, a certain filter may work excellently for a certain type of images, but may not be suitable for other images. Thus, the selection of filters is exceedingly important in practice. Moreover, if a filter includes adjustable parameters such as the regularization parameter or threshold, its restoration performance relies heavily on the choice of the parameter values [5]. It is a common

\* Corresponding author. Tel.: +370 69822456; fax: +370 37330446.

E-mail addresses: [minvydas.ragulskis@ktu.lt](mailto:minvydas.ragulskis@ktu.lt), [algimantas.aleksa@ktu.lt](mailto:algimantas.aleksa@ktu.lt)

(M. Ragulskis), [rimas.maskeliunas@me.vgtu.lt](mailto:rimas.maskeliunas@me.vgtu.lt) (R. Maskeliunas).

<sup>1</sup> Tel./fax: +370 52744736.

understanding that one filter will not outperform all other filters, in all situations.

Thus, moving average filter development remains an active research area. Novel moving average filters are used for calculating local statistics in polygonal shaped windows in real-time applications [6], for modeling stochastic and structured textures [7], for ultrasound image processing [8], for noise reduction in color images [9], for moving object detection from color video sequences [10] and for many other different applications.

In this paper, we propose a new moving average, nonlinear, single stage, space invariant filter for visualization of fringes in time-averaged projection moiré images. The filter window must be oriented in a direction perpendicular to constitutive lines of the projected moiré grating. Moreover, a whole number of pitches of the projected grating must fit into the filter window. Failure to fulfill these requirements for the filter window may compromise the functionality of the filter. The estimation operation is a nonlinear fringe mapping function, described in detail in Section 3, while Section 2 gives an overview on the formation of fringes in optical projection moiré. The adjustment of filter parameters is discussed in Section 4. Applicability of the filter for experimental optical moiré images is illustrated in Section 5. Concluding remarks are given in the last Section.

## 2. Optical background

Advanced strain measurement and control tools (including geometric moiré techniques) are regarded as primary technology drivers in such industries as MEMS (micro-electro-mechanical systems) fabrication and high-precision machine tools manufacturing [11–13]. Accurate interpretation of experimental measurement results is one of the crucial factors enabling minimization of the general uncertainty budget.

Geometric moiré [14,15] is a classical in-plane whole field non-destructive optical experimental technique based on analysis of visual patterns produced by superposition of two regular gratings that geometrically interfere. Examples of gratings are equispaced parallel lines, concentric circles, and arrays of dots. The gratings can be superposed by double-exposure photography, by reflection, by shadowing, or by direct contact [16,17]. Moiré patterns are used to measure variables such as displacements, rotations, curvature, and strain throughout the viewed area. In-plane moiré is typically conducted with gratings of equispaced parallel lines [15,16].

One-dimensional example is analyzed for simplicity at first. Moiré grating on the surface of a one-dimensional structure in the state of equilibrium can be interpreted as a periodic variation of black and white colors

$$M_1(x) = \frac{1}{2} \left( 1 + \cos\left(\frac{2\pi}{\lambda}x\right) \right) = \cos^2\left(\frac{\pi}{\lambda}x\right) \quad (1)$$

where  $x$  is the longitudinal coordinate;  $M_1$  is grayscale level of the surface at point  $x$ ; and  $\lambda$  the pitch of the grating. Numerical value 0 of the function in Eq. (1) corresponds to black color; 1—to white color; all intermediate values—to grayscale levels.

The grating of one-dimensional structure in a deformed state can be interpreted as follows:

$$M_2(x) = \cos^2\left(\frac{\pi}{\lambda}(x - u(x))\right) \quad (2)$$

where  $u(x)$  is slowly varying deformation of the original grating at point  $x$  [14,15].

Additive superposition [15] of the original and the deformed gratings yields

$$\begin{aligned} M_{12}(x, u(x)) &= \frac{1}{2} \left( \cos^2\left(\frac{\pi}{\lambda}x\right) + \cos^2\left(\frac{\pi}{\lambda}(x - u(x))\right) \right) \\ &= \frac{1}{2} + \frac{1}{2} \cos\left(\frac{2\pi}{\lambda}\left(1 - \frac{u(x)}{2x}\right)x\right) \cos\left(\frac{\pi}{\lambda}u(x)\right). \end{aligned} \quad (3)$$

Fringes will form at the centers of beatings where

$$\cos\left(\frac{\pi}{\lambda}u(x)\right) = 0. \quad (4)$$

Eq. (4) yields the relationship between fringe order, deformation and pitch of the grating [14,15]

$$u(x) = \lambda \left( n - \frac{1}{2} \right) \quad (5)$$

where  $n$  is the fringe order which is determined from the pattern of fringes using automatic, semiautomatic or even manual fringe counting techniques [14].

Double-exposure geometric moiré techniques can be extended to time average geometric moiré methods when the moiré grating is formed on the surface of elastic oscillating structure and time averaging techniques are used for registration of time-averaged patterns of fringes [18]. Time average moiré is exploited in numerous engineering applications involving time average projection, reflection, and geometric moiré [19–21].

Again, we will use one-dimensional model to illustrate the formation of time-averaged fringes. We assume that the deflection from state of equilibrium varies in time

$$u(x, t) = u(x) \sin(\omega t + \varphi) \quad (6)$$

where  $\omega$  is cyclic frequency,  $\varphi$  is phase, and  $u(x)$  the amplitude of oscillation at point  $x$ . Then time-averaged grayscale level can be expressed like [18,21]

$$\begin{aligned} M_T(x) &= \lim_{T \rightarrow \infty} \frac{1}{T} \int_0^T \cos^2\left(\frac{\pi}{\lambda}(x - u(x) \sin(\omega t + \varphi))\right) dt \\ &= \frac{1}{2} + \frac{1}{2} \cos\left(\frac{2\pi}{\lambda}x\right) \lim_{T \rightarrow \infty} \frac{1}{T} \int_0^T \exp\left(i \frac{2\pi}{\lambda}u(x) \sin t\right) dt \\ &= \frac{1}{2} + \frac{1}{2} \cos\left(\frac{2\pi}{\lambda}x\right) J_0\left(\frac{2\pi}{\lambda}u(x)\right). \end{aligned} \quad (7)$$

where  $T$  is exposure time;  $i$  the imaginary unit;  $J_0$  the zero-order Bessel function of the first kind. Time-averaged fringes will form at such  $x$  where  $J_0((2\pi/\lambda)u(x)) = 0$ . Now the relationship between fringe order, deformation and pitch of the grating takes the following form:

$$\frac{2\pi}{\lambda}u_i(x) = r_i \quad (8)$$

where  $r_i$  denotes  $i$ -th root of the zero-order Bessel function of the first kind;  $u_i$  is the amplitude of oscillation at the center of the  $i$ -th fringe.

Numerically reconstructed one-dimensional moiré gratings in Fig. 1 illustrate the formation of double-exposure and time-averaged fringes: Fig. 1(a) illustrates moiré grating in state of equilibrium; Fig. 1(b)—deformed moiré grating when  $u(x) = kx$ ;  $k = 0.05$ ; Fig. 1(c) represents the effect of beatings produced by additive superposition of Fig. 1(a) and (b) (Eq. (3)); Fig. 1(d) shows time-averaged fringes when the dynamic deflections from the state of equilibrium oscillate in time (Eq. (7);  $u(x) = kx$ ;  $k = 0.05$ ).

It must be noted that the grayscale level at the centers of moiré fringes produced both by additive superposition and time averaging is equal to 0.5 (Eqs. (3) and (7)). But the peak level between adjacent time-averaged fringes drops down with the increase of dynamic amplitude (Fig. 1(d)). That can be explained by the properties of the zero-order Bessel function of the first kind:  $\lim_{x \rightarrow +\infty} J_0(x) = 0$ . Therefore, analysis of time-averaged

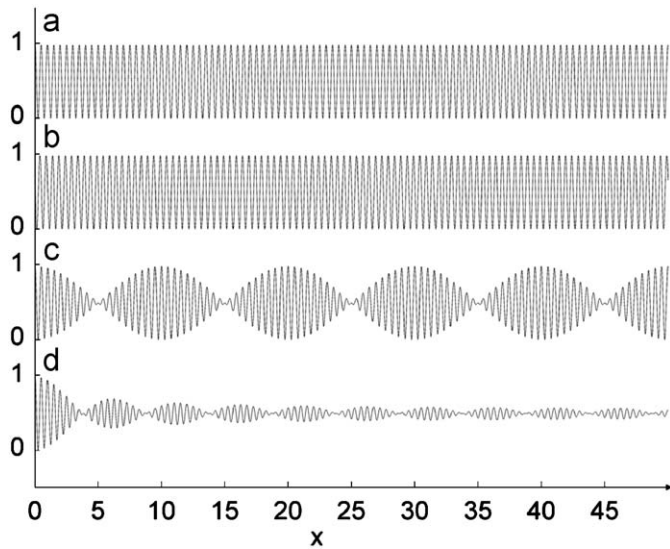


**Fig. 1.** Formation of time-averaged moiré fringes: (a) moiré grating in state of equilibrium; (b) deformed moiré grating ( $u(x) = kx$ ;  $k = 0.05$ ); (c) moiré fringes produced by additive superposition of digital images in (a) and (b); and (d) time-averaged moiré fringes ( $u(x) = kx$ ;  $k = 0.05$ ).

fringes (especially, higher-order fringes) in digital images produced by experimental investigations usually comprise digital image filtering techniques [22–24]. We will shortly overview these techniques in the following section.

### 3. Contrast enhancement of time-averaged moiré fringes

Classical contrast enhancement techniques applicable for patterns of time-averaged moiré fringes comprise two basic steps [25]. First, the digital image is filtered using grayscale level adjustment transformation where levels around 0.5 are mapped to 0 (middle gray levels are mapped to black color); all other grayscale levels are mapped to 1 (grayscale levels except middle gray are mapped to white color). The second step is application of morphological operations to eliminate parasitic interference lines generated by high special frequency components originating from the initial moiré grating.

This image transformation is illustrated in Fig. 2 (label (d) corresponds to time average moiré image from Fig. 1(d)). It can be noted that applicability of phase-stepping techniques [26] for visualization of time average moiré fringes cannot be used directly, because grayscale level at moiré fringe centerlines is 0.5 (not 0 as for time-averaged fringes produced by laser holography [27]).

The mapping function  $F(M(x,y))$  used for contrast enhancement must satisfy several basic requirements:

- (i)  $F: [0,1] \rightarrow [0,1]$ ;
- (ii)  $F(m) = 0$ ;
- (iii)  $F: [m-\varepsilon, m+\varepsilon] \rightarrow [0, \delta]$  or alternatively,  $F: [0, m-\varepsilon] \cup [m+\varepsilon, 1] \rightarrow [1-\delta, 1]$ ;  $\varepsilon, \delta > 0$ ;  $0 < m < 1$ ; and
- (iv)  $F(\xi) = F(2m - \xi)$ ;  $\xi \in [0, 1]$ .

(9)

The second condition requires that the mapped grayscale color at the centerline of time-averaged fringe must be black ( $m = 0.5$  for time average geometric moiré). The third condition requires that levels in a  $2\varepsilon$  bandwidth around  $m$  are mapped to grayscale levels not higher than  $\delta$  (dark color), or alternatively, the levels outside  $2\varepsilon$  band around  $m$  are mapped to levels not lower than  $1-\delta$  (bright color). The fourth requirement necessitates that the

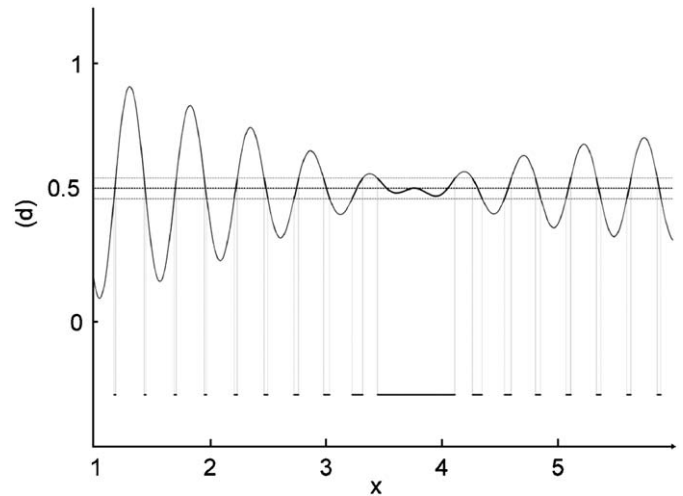


**Fig. 2.** Contrast enhancement of time-averaged fringes: dashed lines represent the bandwidth of grayscale levels mapped to the black color; the bottom line diagram stands for the enhanced one-dimensional image.

mapping function is symmetric in respect to  $m$  ( $\xi$  is the grayscale level).

Many mapping functions satisfy the up-mentioned requirements; we will mention few functions.

Step mapping function

$$F(M(x,y)) = \begin{cases} 0, & \text{when } m - \varepsilon \leq M(x,y) \leq m + \varepsilon \\ 1, & \text{elsewhere} \end{cases}$$

Characteristic feature of step mapping function is that the continuous grayscale interval is mapped into pure black and white colors. This feature can be advantageous in certain applications, especially when subsequent morphological operations are used (it can be easier to manipulate with only black and white pixels). The drawback is the problematic location of the fringe centers in the mapped image. Even very small  $\varepsilon$  will not eliminate parasitic fringes from the mapped image (true fringes will be also thin then). Subsequent morphological operations can wipe out not only parasitic but also true fringes. Pencil mapping function

$$F(M(x,y)) = \begin{cases} \frac{1}{\varepsilon} |M(x,y) - m|, & \text{when } m - \varepsilon \leq M(x,y) \leq m + \varepsilon \\ 1, & \text{elsewhere} \end{cases}$$

Pencil mapping functions are advantageous when centerlines of time-averaged fringes are to be determined. The drawback is associated with problematic applicability of morphological operations for wiping out parasitic fringes. Potential of pencil functions can be fully revealed when step functions are used to enhance the time-averaged image. Initially, parasitic fringes are wiped out and then the produced pattern is used as a mask to reconstruct the original grayscale levels (only in the regions of mapped black fringes). The pencil function then can be effectively used to reconstruct fringe centerlines in the region-of-interest portions of the original image.

Square of sigmoidal function

$$F(M(x,y)) = \tanh^2(k(M(x,y) - m))$$

Hyperbolic tangent and square of hyperbolic tangent are widely used in neural networks and image processing [28]. Coefficient  $k$  determines the sharpness of the mapped fringe [29]. Application of this function is advantageous in the sense that the mapped image does not have any sharp boundaries (square of hyperbolic tangent is a continuous function). Nevertheless, it does not eliminate the problem of parasitic fringes. Moreover, wiping out

of parasitic fringes can be even more complex compared to step functions.

#### 4. Time average projection moiré and problems of contrast enhancement

Projection moiré [14] is an effective experimental technique exploiting similar optical principles as geometric moiré. The main advantage of this technique is that moiré grating is formed by projecting an array of grayscale lines onto the surface of the deformable body instead of physically drawing these lines. That feature is very important in such applications where graphical formation of grating lines is complicated or even impossible.

Such situation occurs when one needs to measure paper vibrations in a printing machine where paper band rolls at relatively high speeds. Experimental setup comprises a PC, digital camera, projector, and the object itself. A digital image of an array of dark and white stripes is projected onto the surface of the rolling paper band (Fig. 3). By the way, moiré grating must be projected obliquely—the projected grating lines will not deform if the incident light would be orthogonal to the object's surface (even when the object's surface will deform) [14]. The paper band rolls during the exposure time which is long enough (3 s in our experiments) to accommodate sufficiently large number of high-frequency paper vibration periods (in the transverse direction).

The basic optical principles governing the formation of fringes produced by time average projection moiré are generally the same compared to time average geometric moiré [14]. Though double-exposure projection moiré is a well-established experimental technique with numerous practical applications, interpretation of patterns of fringes produced by time average projection moiré is an open problem and depends heavily on the quality of the registered time-averaged fringes. Clearly, the decay of illumination of fringes at increasing fringe orders produced by time average projection moiré requires exploitation of digital image processing techniques (Fig. 4).

As mentioned previously, it is quite hard to note any time-averaged fringes in Fig. 4 by a naked eye. Nevertheless, digital contrast enhancement techniques based on the fact the time-averaged fringe form around the grayscale values of  $m = 0.5$  do not produce satisfactory results either (Fig. 5). That can be explained by a simple reason that the grating lines are projected in an oblique angle ( $30^\circ$  from the perpendicular direction in our experimental setup; Fig. 3). As the distance between the projector



Fig. 3. General view of the experimental setup.

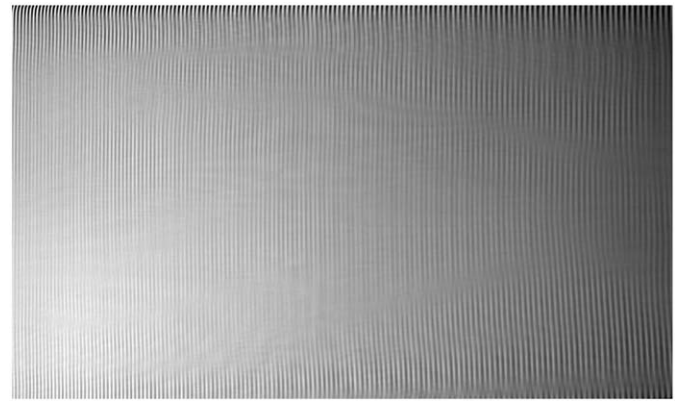


Fig. 4. Pattern of time-averaged fringes in a digital image produced by time average projection moiré.

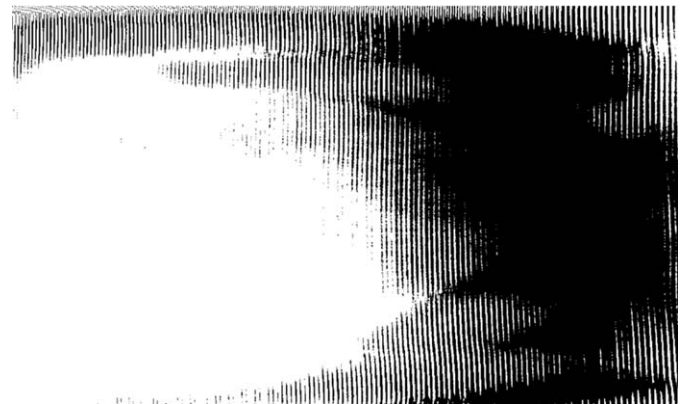


Fig. 5. Results produced by contrast enhancement of digital image in Fig. 4 (step mapping function;  $m = 0.5$ ;  $\varepsilon = 0.15$ ).

and the surface is comparable to the dimension of the surface itself, the distance from the projector's lens to the left part of the surface is smaller than to the right part of the surface. Thus, the illumination at different parts of the surface is different (Fig. 4). One can try to change the value of  $m$  and the mapping function used, but the produced results are really not better than shown in Fig. 5. Naturally, such results cannot be used by a professional experimentalist who would try to use reverse engineering techniques linking fringe numbers with the magnitudes of dynamic displacements. Probably, the difficulties with the interpretation of time-averaged projected fringes is one of the factors why time average projection moiré is much less popular experimental technique compared to time average geometric moiré where moiré grating is physically imprinted onto the surface of analyzed body [14].

#### 5. Contrast enhancement of time-averaged fringes using moving average method

The fact that the illumination of the surface is not uniform poses a certain requirement for contrast enhancement techniques used to visualize the pattern of time-averaged fringes. One needs to use different values of  $m$  (Eq. (9)) at different parts of the digital image. We propose a moving average method for automatic identification of parameter  $m$  and subsequent mapping of grayscale levels at appropriate pixels. This technique comprises the following basic steps:

- (i) Identification of direction orthogonal to the constitutive moiré grating lines.
- (ii) Identification of the number of pixels fitting into one pitch of the time-averaged image.
- (iii) Calculation of average grayscale color  $m$  at zone of interest.
- (iv) Mapping appropriate pixels by selected mapping function.

We will illustrate every step of this technique applying contrast enhancement of digital image presented in Fig. 4.

It is well known that moiré techniques are sensitive to deflections in the direction orthogonal to the constitutive moiré grating lines [14]; therefore, we require that contrast enhancement technique must exploit this phenomenon. Moiré grating lines are vertical in our experimental setup (Fig. 4), so the direction of analysis is horizontal. If moiré grating lines would be oblique, one would need to use inclined direction of analysis (what it really not a drawback of this technique since digital images can be readily sliced and approximated in different cut directions).

More demanding step if the identification of the number of pixels fitting into one pitch of the time-averaged image. This is more or less manual procedure and is illustrated in Fig. 6. In our example this number is 6. If the ratio between the pitch and the pixel width is not a whole number, two or even three pitches can be considered as a window length used for calculation of average grayscale color  $m$  in that part of the digital image. Such reconstruction of parameter  $m$  is performed independently for every pixel line. Moving average is constructed only for pixel row, not column.

The next step is the implementation of the moving average method itself. It is illustrated in Fig. 7. The top pixel row represents  $i$ -th pixel line in the original digital image (it is of course shortened for clarity in Fig. 7). Initially, the first six leftmost pixels are considered (step 1, Fig. 7). Grayscale color average is calculated in this window and is represented as a background color in pixel labeled as 1 in Fig. 7. This average grayscale level is assumed as the current value of parameter  $m$  (Eq. (9)). Now, the selected mapping function is employed for the middle pixel of the current window (this is illustrated by the arrow line connecting the averaged pixel and the processed pixel in Fig. 7). As the window's width is 6 (in our example), we selected the third pixel as the pixel which is processed by the mapping function. The bottom line in Fig. 7 represents the contrast-enhanced pixel line. It appears that the third pixel in the original pixel line is mapped to black color (in the contrast-enhanced pixel line). The first two crosses on the left stand for the fact that we

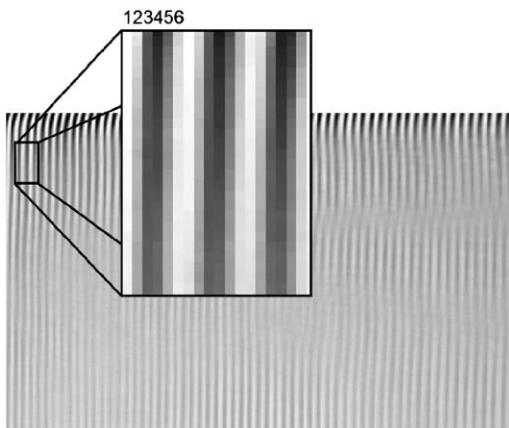


Fig. 6. Identification of grating's pitch in terms of pixels.

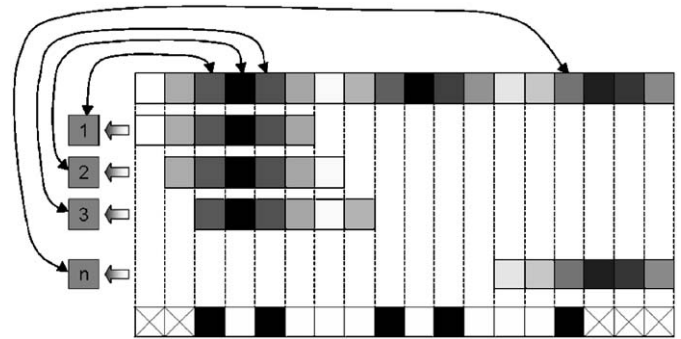


Fig. 7. Schematic diagram of contrast enhancement algorithm based on moving average technique.

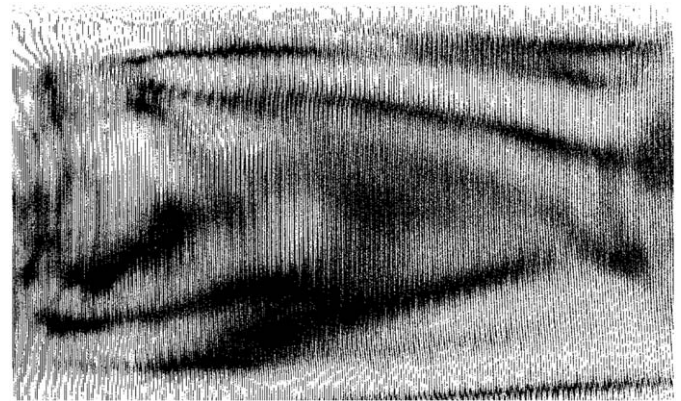


Fig. 8. Results produced by contrast enhancement of digital image in Fig. 4 (moving average algorithm; step mapping function;  $\epsilon = 0.03$ ).

cannot go more left with the window than the leftmost side of the original line of pixels.

The next step is to shift the window to the right by one pixel. This is illustrated by the third pixel row in Fig. 7. The shift is executed into the right side; not to the bottom. The process is continued until the window reaches the right side of the original pixel line. Finally, such mapping process is executed for all lines of the original image. The produced digital image is presented in Fig. 8. Moving average technique copes well with variable background illumination—the digital image in Fig. 8 is incomparable with Fig. 5. It can be noted that digital image in Fig. 8 is a black and white (not grayscale) image, because we used step mapping function for contrast enhancement.

Nevertheless, moving average contrast enhancement technique does not eliminate the problem of parasitic fringes (Fig. 2), but the pattern of time-averaged projection fringes is clearly visible in Fig. 8. Pixel-based morphological operations (pixel's neighbors' count-and-eliminate method) [30] can be used to eliminate parasitic fringes. But experienced optical engineers already can understand the physical processes taking place in the rolling paper band and use fringe counting techniques [31] to determine the magnitudes of dynamic displacements from Fig. 8.

## 6. Concluding remarks

A new moving average-based contrast enhancement technique for visualization of time-averaged fringes in digital images produced by time average projection moiré is proposed in this paper. This technique copes well with the problem of variable grayscale levels at centerlines of the fringes. This method has a potential for applicability in automatic or semiautomatic fringe

counting techniques used for analysis of patterns of fringes in images with not uniform illumination.

## References

- [1] Tukey JW. Exploratory data analysis. Reading, MA: Addison Wesley; 1971.
- [2] Dougherty ER. An introduction to morphological image processing. SPIE Press; 1992.
- [3] Pavlidis T. Algorithms for graphics and image processing. Rockville: Computer Science Press Inc.; 1982.
- [4] Niblack W. An introduction to digital image processing. London: Prentice-Hall International (UK) Ltd.; 1986.
- [5] Sugiyama M, Ogawa H. A unified method for optimizing linear image restoration filters. *Signal Processing* 2002;82:1773–87.
- [6] Sun Changming. Moving average algorithms for diamond, hexagon, and general polygonal shaped window operations. *Pattern Recognition Letters* 2006;27:556–66.
- [7] Eom KB. 2-D moving average models for texture synthesis and analysis. *IEEE Transactions on Image Processing* 1998;7:1741–6.
- [8] Morales-Mendoza LJ, Shmaliy Y, Ibarra-Manzano OG, Arceo-Miquel LJ, Montiel-Rodriguez M. Moving Average Hybrid FIR Filter in Ultrasound Image Processing. In: *Proceedings of the 18th International Conference on Electronics, Communications and Computers*; IEEE Computer Society Washington, DC, USA, 2008; p. 160–4.
- [9] Shinya K. Color image processing apparatus executing moving-average processing for noise reduction in color image signals, United States Patent 6980335, 2005.
- [10] Zhang Xiang, Yang Jie. The analysis of the color similarity problem in moving object detection. *Signal Processing* 2009;89:685–91.
- [11] Shang H, Xie H, Wang X, Jiang S, Dai F, Wang W, et al. Thermal properties measurement of micro-electromechanical system sensors by digital moiré method. *Strain* 2005;41:157–62.
- [12] Han A. Recent advancements of moiré and microscopic moiré interferometry for thermal deformation analyses of microelectronics devices. *Experimental Mechanics* 1998;38:278–88.
- [13] Sciammarella CA, Sciammarella FM, Kim T. Strain measurements in the nanometer range in a particulate composite using computer-aided moiré. *Experimental Mechanics* 2003;43:341–7.
- [14] Kobayashi AS. Handbook on experimental mechanics. 2nd ed. Bethel: SEM; 1993.
- [15] Patorski K, Kujawinska M. Handbook of the moiré fringe technique. Amsterdam: Elsevier; 1993.
- [16] Post D, Han B, Ifju P. High sensitivity moiré: experimental analysis for mechanics and materials. Berlin: Springer; 1997.
- [17] Dai FL, Wang ZY. Geometric micron moiré. *Optics and Lasers in Engineering* 1999;31:191–8.
- [18] Liang CY, Hung YY, Durelli AJ, Hovanesian JD. Time-averaged moiré method for in-plane vibrational analysis. *Journal of Sound and Vibration* 1979;62:267–75.
- [19] Mitchell AK. Optical modal analysis using white-light projected fringes. *Experimental Mechanics* 2005;45:250–8.
- [20] Asundi A. Novel techniques in reflection moiré. *Experimental Mechanics* 1994;34:230–42.
- [21] Ragulskis M, Maskeliunas R, Ragulskis L, Turla V. Investigation of dynamic displacements of lithographic rubber roller by time average geometric moiré. *Optics and Lasers in Engineering* 2005;43:951–62.
- [22] Cai LZ, Liu Q, Yang XL. A simple method of contrast enhancement and extremum extraction for interference fringes. *Optics & Laser Technology* 2003;35(4):295–302.
- [23] Huang MJ, Zi-Neng He, Feng-Zheng Lee. A novel methodology for enhancing the contrast of correlation fringes obtained by ESPI. *Measurement* 2004;36(1):93–100.
- [24] Murukeshan VM, Lai Yin Fei, Krishnakumar V, Ong LS, Asundi A. Development of Matlab filtering techniques in digital speckle pattern interferometry. *Optics and Lasers in Engineering* 2003;39(4):441–8.
- [25] Soille P. Morphological phase unwrapping. *Optics and Lasers in Engineering* 2000;32(4):339–52.
- [26] Chan PH, Bryanston-Cross PJ, Parker SC. Spatial phase stepping method of fringe-pattern analysis. *Optics and Lasers in Engineering* 1995;23(5):343–54.
- [27] West CM. Holographic interferometry. New York: Wiley; 1979.
- [28] Cancelliere R, Gai M. A comparative analysis of neural network performances in astronomical imaging. *Applied Numerical Mathematics* 2003;45(1):87–98.
- [29] Ragulskis M, Saunoriene L. Applicability of optical geometric differentiation for time-average geometric moiré. *Strain* 2006;42(3):173–9.
- [30] Terol-Villalobos IR, Mendiola-Santibáñez JD, Canchola-Magdalenos SL. Image segmentation and filtering based on transformations with reconstruction criteria. *Journal of Visual Communication and Image Representation* 2006;17(1):107–30.
- [31] Von Martens H-J. Generalization and analysis of the fringe-counting method for interferometric measurement of motion quantities. *Measurement* 1999;25(1):71–87.